Desalination and Water Treatment
www.deswater.com
doi: 10.5004/dwt.2021.27282

226 (2021) 441–451
June

Application of response surface methodology for optimization of methylene blue adsorption onto activated carbons prepared from chestnut shell

Mingyang Zhang[a,*], Xinzhe Liu[a], Wenda Li[a], Lili Guo[a], Zhuowei Tan[b], Qian Wang[a], Linhua Zhang[a,*]

[a]*School of Thermal Engineering, Shandong Jianzhu University, Jinan 250101, Shandong, China, Tel./Fax: +86-531-86367629; emails: zhangmingyang18@sdjzu.edu.cn (M.Y. Zhang), zhth0015@sdjzu.edu.cn (L.H. Zhang), liuxinzheoffice@163.com (X.Z. Liu), 1545697454@qq.com (W.D. Li), 1844264872@qq.com (L.L. Guo), wangqian18@sdjzu.edu.cn (Q. Wang)*
[b]*College of New Energy, China University of Petroleum (East China), 266580, Shandong, China, Tel./Fax: +86-532-86981865; email: tanzhuowei1990@126.com*

Received 22 September 2020; Accepted 1 April 2021

ABSTRACT

In this study, the activated carbons prepared from chestnut shells (CnSACs) were applied for methylene blue (MB) adsorption from aqueous solutions. The surface properties of CnSACs were identified by Brunauer–Emmett–Teller (BET) and scanning electron microscopy analysis. And the N_2 adsorption–desorption isotherms indicate that the CnSACs exhibit Type I isotherms. Besides, response surface methodology in combination with Box–Behnken design was used to optimize the preparation parameters (impregnation mass ratio, impregnation time, activation temperature and activation time). The MB adsorption capacity was used as the response value. The statistical analysis showed that the quadratic model was significant. The R^2 for the model was 0.98 and the adjusted R^2 was 0.97. In addition, the activation temperature was found to have a more significant impact on the MB adsorption due to the highest *F*-value. Moreover, the optimum preparation conditions were found to be impregnation mass ratio of 11.36, impregnation time of 29.17 h, activation temperature of 632.40°C and activation time of 81.390 min. The experimental value of MB adsorption capacity prepared under the optimum preparation parameters was 1,060.94 mg/g with the BET surface area of 1,602.99 m^2/g.

Keywords: Activated carbon; Methylene blue adsorption; Chestnut shell; Response surface methodology; Box–Behnken design

1. Introduction

With the increasing attention paid to environmental protection, the treatment of industrial wastewater has become an urgent problem in various industries. Dyes are one of the major components of wastewater produced from many industries related to textile, paint, tanneries, ink, plastics, and paper [1,2]. Among these industries, the textile industry is the major consumer of dyes and sources of dye wastewater [3]. The statistics show that the losses of reactive dyes are about 11% in the textile industry. Thereby, about 40,000~50,000 tons of dyes are continuously entering the water systems annually [4]. Dye wastewater is characterized by strong biotoxicity, high chrominance, high pH, poor bio-degradability, complex composition and a large amount of suspended solids [5]. Consequently, the dissolved oxygen level in the dye wastewater declines due to the shielding effect of disperse dye molecules on sunlight. Besides, heavy-metal salts such as chromium, lead and mercury in dye wastewater can endanger human health

* Corresponding authors.

through the food chain. Therefore, the removal of dyes from dye wastewater is of vital importance from both viewpoints of environment protection as well as human health [6,7].

The main pollutants of dye wastewater are basic raw materials and their by-products from the reaction, and the pollutants are mainly composed of dyes, slurries, and additives [8]. There is a wide variety of dyes including reactive dye, acidic dye, direct dye, cationic dye, insoluble azo dye and sulfide dye, etc [9]. Methylene blue (MB) is a typical cationic phenothiazines dye, which can be used to make ink, lake, organisms and dye bacterial tissues. Besides, it also can be used for the dyeing of cotton, hemp, silk fabrics, paper, bamboo and wood [10]. However, ingestion of too much MB may cause nausea, vomiting, sweating, mental confusion and dyspnea. Thus, in this paper, the removal of MB from aqueous solutions was used as the laboratory test for the decolorization and biosafety disposal of dye wastewater.

There are many processes available for the color removal from dye wastewater, namely adsorption [11], coagulation [12], chemical oxidation [13], floatation [14], membrane separation [15], ion exchange [16], photochemistry [17], electrochemistry [18], biofilm [19] and anaerobic treatment [20]. Among these treatment methods, adsorption has been considered widely used due to its universality, economy and easy operation. Adsorption is a mass transfer process in which substances in an aqueous solution are adsorbed onto an adsorbent. The commonly used adsorbents are activated carbon, clay, resin, coke, diatomite, nanocomposite and slag [21,22]. However, activated carbon is usually preferred for wastewater treatment for its low cost, simplicity and no-toxic.

Activated carbon (AC) is characterized by high surface area, well-developed pore structure, large adsorption capacities and fast adsorption rate [23,24]. However, the high cost of ACs limits their widespread use in industry. Therefore, the researches of ACs preparation have been focused on the identification of cheaper sources and activation methods. From the perspective of treating waste with waste, various agricultural wastes and forestry products have been used as raw materials for the preparation of ACs. Naushad et al. [25] proposed a modified sodium hydroxide-treated pine nutshell with a surface area of more than 266 m^2/g, and the maximum MB adsorption was found to be 39.73 mg/g. Khan et al. [26] presented an investigation on the biosorption potential of sodium hydroxide treated pistachio shell biomass for MB. The results showed that the Brunauer–Emmett–Teller (BET) surface area of the adsorbent was greater than 35.57 m^2/g. Pérez-Marín et al. [27] used the orange waste as a biosorbent material for the removal of Cd(II) ions from aqueous solutions. The maximum adsorption capacity was found to be 0.43 mmol/g.

In this study, a porous activated carbon prepared from chestnut shell (CnSAC) by the chemical activation ($ZnCl_2$) was used for MB adsorption from aqueous solutions. Based on the previous investigation of the influence of preparation parameters (impregnation mass ratio, impregnation time, activation temperature, activation time) on MB adsorption capacity, the preparation process was optimized using Box–Behnken design (BBD) under response surface methodology (RSM) to establish a model to predict MB adsorption capacity. In addition, the optimum preparation parameters were obtained. Eventually, the surface properties of CnSAC prepared under the optimum preparation conditions were identified by BET and scanning electron microscopy (SEM) analysis. This paper aims to obtain the surface morphology of CnSACs, specify the type of isothermal adsorption and reveal the relationship between preparation parameters and MB adsorption capacity. The rest of the paper is organized as follows. The preparation of CnSACs and experimental design are discussed in the next section. The characterization of CnSACs, regression analysis and the optimization of preparation parameters are presented in Section 3. Finally, the paper closes with a summary of the results in the last section.

2. Experimental

2.1. Materials and characterization

The MB ($C_{16}H_{18}ClN_3S{\cdot}3H_2O$) used in the experiment was supplied by Tianjin Zhiyuan Chemical Reagent Co., Ltd., (China) with a purity greater than 98.5%. And the chemical structure of MB is shown in Fig. 1. The $ZnCl_2$ was produced by Pingxiang Baishi Chemical Reagent Co., Ltd., (China) with a purity greater than 98.0%.

The stock solution (200 mg/L) of MB was prepared by dissolving 250 mg of MB in 250 mL deionized water and the working concentrations were prepared by its dilution. The MB concentration measurement was carried out using an ultraviolet spectrophotometer (model T6, Pgeneral, China) at a wavelength of 665 nm. The surface morphology of CnSACs was analyzed by scanning electron microscope (SEM, Hitachi S-4800, 7593-H, Japan). And the surface area of CnSACs was calculated from the BET method and pore size distributions were measured using Autosorb iQ.

2.2. Preparation of CnSAC

Firstly, about 2 g of the chestnut shell was dried for 24 h in an air-dry oven. Then, it was grounded in a grinder and sieved (200 mesh). Secondly, the powder was impregnated in 25 wt.% $ZnCl_2$ aqueous solution with the mass ratio was 12.5:1 ($ZnCl_2$ aqueous solution to chestnut shell powder) for 27 h. And then, the mixture was carbonized in a tube furnace at 600°C under a nitrogen atmosphere for 75 min with a heating rate of 10°C/min. Finally, the cooled carbonation products were washed thoroughly with deionized water and dried at 102°C for 24 h. Thus the porous activated carbon prepared from chestnut shell (CnSAC) was obtained.

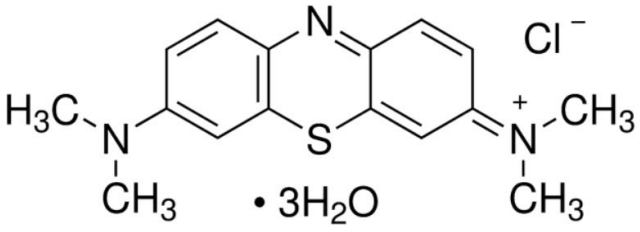

Fig. 1. Chemical structure of MB.

2.3. Box–Behnken design

RSM is a collection of statistical and mathematical techniques, which is used to model and reveal the relationship between independent variables and response variables [28,29]. Based on the results of multiple linear regression, a regression equation with a good fitting degree is obtained, and a multidimensional space surface is established. Besides, a reasonable experimental design can permit simultaneous optimization of variables and minimize error with the minimum number of runs. In this paper, the experiments for MB adsorption capacity of CnSACs were designed using BBD with four factors, that is, impregnation mass ratio (A, i_r), impregnation time (B, i_t), activation temperature (C, a_{tp}) and activation time (D, a_{tm}) using Design-Expert 10.0 with 29 runs. BBD is a second-order experimental design method based on three levels [30]. Compared with other design methods, it is characterized by fewer times experiments and higher efficiency. Table 1 shows the designed experimental parameters together with experimental results. The independent variables with the low and high levels were coded as –1 and +1, respectively.

3. Results and discussion

3.1. Characterization of the CnSACs

The N_2 equilibrium adsorption isotherm of two typical CnSACs (No. 1 and No. 2) at 77.35 K is shown in Fig. 2. The preparation parameters of the two typical CnSACs are shown in Table 2. It can be seen that the nitrogen volume adsorbed increases firstly (P/P_0 < 0.4)

Table 2
Preparation parameters of the two typical CnSACs

Samples	i_r	i_t (h)	a_{tp} (°C)	a_{tm} (min)
No. 1	12.5	27	550	90
No. 2	10	24	600	75

Table 1
Designed experimental parameters

No.	i_r		i_t (h)		a_{tp} (°C)		a_{tm} (min)		MB adsorption q_e (mg/g)
	A	code	B	code	C	code	D	code	
1	12.5	0	27	0	650	1	60	–1	936.47
2	10	–1	27	0	600	0	90	1	967.67
3	10	–1	27	0	550	–1	75	0	906.71
4	10	–1	24	–1	600	0	75	0	947.83
5	15	1	27	0	650	1	75	0	934.02
6	12.5	0	27	0	600	0	75	0	1,026.48
7	12.5	0	30	1	600	0	60	–1	920.70
8	12.5	0	27	0	600	0	75	0	1,026.48
9	15	1	30	1	600	0	75	0	916.80
10	10	–1	27	0	600	0	60	–1	903.57
11	12.5	0	27	0	550	–1	90	1	873.90
12	12.5	0	24	–1	600	0	90	1	895.92
13	12.5	0	27	0	600	0	75	0	1,026.48
14	10	–1	30	1	600	0	75	0	979.48
15	15	1	27	0	600	0	60	–1	915.15
16	12.5	0	27	0	650	1	90	1	971.61
17	12.5	0	27	0	600	0	75	0	1,026.48
18	12.5	0	30	1	550	–1	75	0	901.59
19	12.5	0	27	0	600	0	75	0	1,026.48
20	12.5	0	24	–1	600	0	60	–1	957.30
21	15	1	27	0	550	–1	75	0	906.21
22	12.5	0	30	1	650	1	75	0	1,024.60
23	12.5	0	27	0	550	–1	60	–1	888.51
24	12.5	0	24	–1	550	–1	75	0	908.41
25	12.5	0	24	–1	650	1	75	0	948.38
26	15	1	24	–1	600	0	75	0	928.94
27	10	–1	27	0	650	1	75	0	993.69
28	12.5	0	30	1	600	0	90	1	995.56
29	15	1	27	0	600	0	90	1	893.13

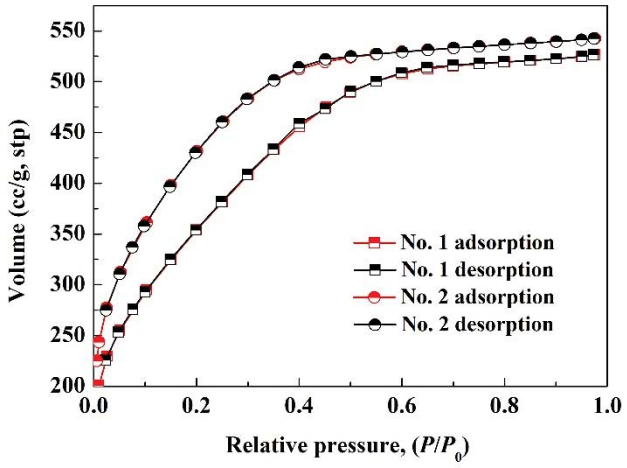

Fig. 2. N_2 adsorption isotherms of CnSACs.

and then tends to be stable (P/P_0 > 0.4) with the increase of relative pressure. The results indicate that both typical CnSACs exhibited Type I isotherms, which means that N_2 molecules are adsorbed mainly in the microporous structure. Therefore, more N_2 is adsorbed due to the pore-filling mechanism [31,32]. Moreover, the BET surface area analysis of the typical CnSACs is shown in Table 3. The results show that the specific surface area of the typical CnSACs based on the BET surface area analyzer is 1,268.62 and 1,524.65 m^2/g, respectively. Besides, the average pore diameter based on the DFT method is 2.59 and 2.21 nm, correspondingly.

The pore size distributions and accumulative pore volume vs. pore width of the typical CnSACs using the DFT method are shown in Fig. 3. The pore size distributions show that the pore size is in the range of 0–3 nm. The results indicate that more micropores on the precursor are developed under the action of $ZnCl_2$ which greatly enriches the diversity of pore structure. Indeed, the characteristics of the pore structure also can explain the results that the adsorption is dominated by micropores in N_2 equilibrium adsorption. Moreover, the SEM micrographs of the typical CnSACs are presented in Fig. 4. The images show that there are abundant abnormity protrusions, depressions and folds on the surface of CnSACs, which

Table 3
BET analysis of the typical CnSACs

	No. 1	No. 2
Multi-point BET		
Correlation coefficient	0.9997	0.9994
C constant	117.27	155.11
Surface area	1,268.62 m^2/g	1,524.65 m^2/g
DFT method		
Average pore diameter	2.59 nm	2.21 nm

results in considerable specific surface area of CnSACs and provides more adsorption sites for the adsorbate.

3.2. Development of regression model equation

To establish a correlation model between the preparation parameters and MB adsorption capacity, Box–Behnken design–response surface methodology with the center point per block of 5 was used. The parameters of the sequential model are summarized in Table 4, which includes the sum of squares, lack of fit tests and model summary statistics. The results show that a quadratic model is suggested for the MB adsorption onto CnSACs. In addition, regression analysis was performed to fit the response function of MB adsorption onto CnSACs. The final quadratic model preferred to calculate the MB adsorption is given by Eq. (1), where the variables take their coded values (–1, 0, 1), represents the MB adsorption (q_e) as a function of impregnation mass ratio (A), impregnation time (B, h), activation temperature (C, °C) and activation time (D, min).

$$q_e(\text{mg/g}) = 1{,}026.48 - 17.06A + 12.66B + 35.29C + 6.34D - 10.95AB - 14.79AC - 21.53AD + 20.76BC + 34.06BD + 12.44CD - 48.10A^2 - 31.56B^2 - 47.98C^2 - 57.31D^2 \quad (1)$$

where the negative signs indicate antagonistic effects and positive signs indicate synergistic effects.

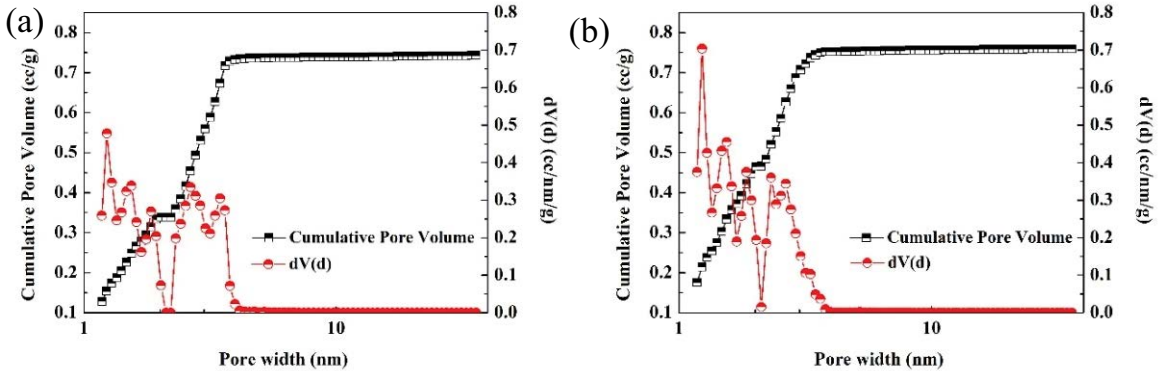

Fig. 3. Pore size distribution and accumulative pore volume curve (a) No. 1 and (b) No. 2.

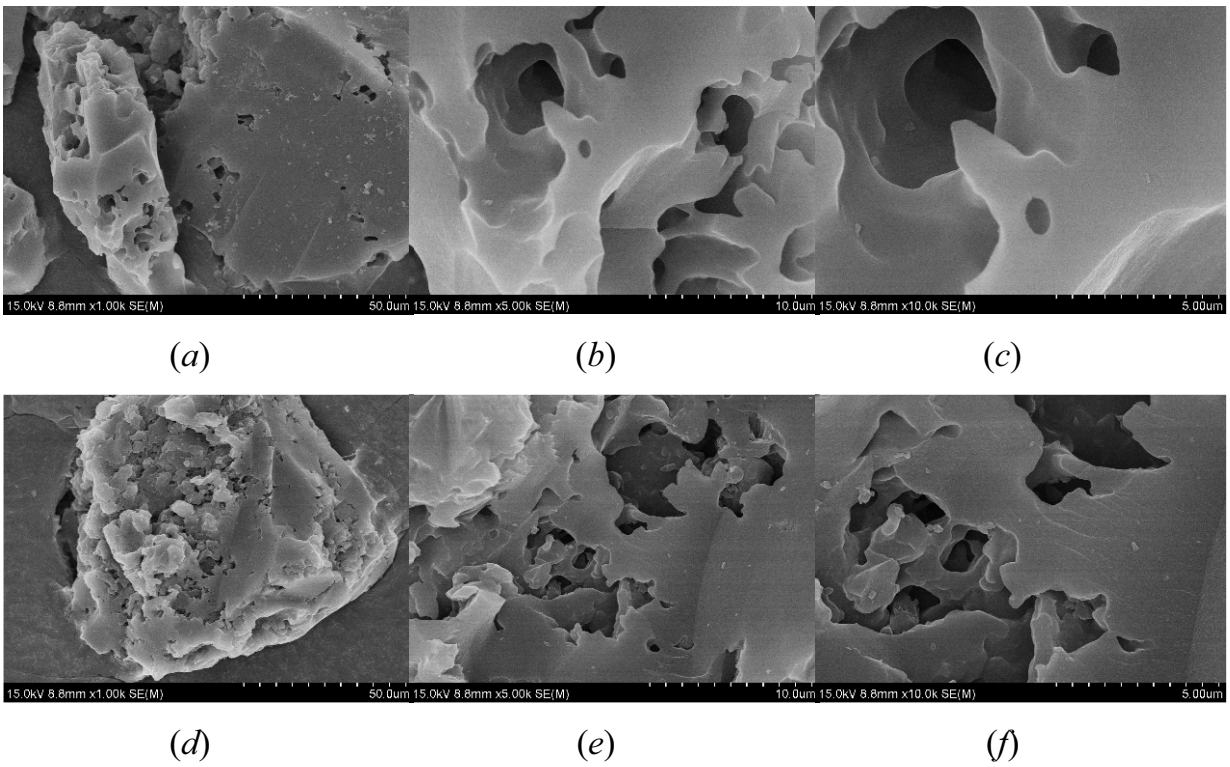

Fig. 4. SEM images of the typical CnSAC: (a–c) No. 1 and (d–f) No. 2.

Table 4
Summary table of the fitted sequential model

Sequential model sum of squares (Type I)						
Source	Sum of squares	df	Mean square	*F*-value	*p*-value Prob. > *F*	
Mean vs. total	2.62×10^7	1	26,169,745			
Linear vs. mean	20,840.17	4	5,210.04	2.53	0.067	
2FI vs. linear	10,191.84	6	1,698.64	0.78	0.60	
Quadratic vs. 2FI	38,141.94	4	9,535.49	117.16	<0.0001	Suggested
Cubic vs. quadratic	845.33	8	105.67	2.16	0.18	Aliased
Residual	294.07	6	49.01			
Total	2.62×10^7	29	904,829.6			
Lack of fit tests						
Linear	49,473.18	20	2,473.66			
2FI	39,281.34	14	2,805.81			
Quadratic	1,139.40	10	113.94			
Cubic	294.07	2	147.04			
Pure error	0.000	4	0.000			

Model summary statistics						
Source	Std. Dev.	*R*-Squared	Adjusted *R*-Squared	Predicted *R*-Squared	PRESS	
Linear	45.40	0.30	0.18	0.10	63,049.40	
2FI	46.72	0.44	0.13	0.081	64,600.23	
Quadratic	9.02	0.98	0.97	0.91	6,562.96	Suggested
Cubic	7.00	0.996	0.98	0.40	42,346.55	Aliased

3.3. Statistical analysis

Based on the correlation coefficient value, the quality of the developed quadratic model was evaluated as shown in Table 4. The adjusted *R*-Squared indicates a measure of the amount of variation about the mean explained by the quadratic model, while the predicted *R*-Squared is a measure of how good the model predicts response data [33]. As shown in Table 4, the *R*-Squared, adjusted *R*-Squared and predicted *R*-Squared for Eq. (1) is 0.98, 0.97 and 0.91, respectively. The predicted *R*-Squared of 0.91 is in reasonable agreement with the adjusted *R*-Squared of 0.97 due to the difference between them is less than 0.2. And the standard deviation (Std. Dev.) for the regression model is 9.02. Therefore, it can be concluded that the predicted values are very close to the experimental values.

Moreover, the analysis of variance (ANOVA) was used to justify the significance and adequacy of the regression model. And the results are shown in Table 5, which suggest the significant contribution of the quadratic model with the *p*-value < 0.0001 and *F*-value of 60.71. This means that only a 0.01% chance that "*F*-value" this large could occur due to noise. In general, a term will be considered with a significant effect if it has a *p*-value less than 0.05 [34]. Thus, in this case, *A*, *B*, *C*, *D*, *AB*, *AC*, *AD*, *BC*, *BD*, *CD*, A^2, B^2, C^2, D^2 are significant model terms as shown in Table 5.

In addition, Fig. 5a shows the comparison between predicted values and the experimental values for MB adsorption capacity. It can be seen that the predicted values are quite close to the experimental values, which indicates intuitively that the developed regression model is successful in elucidating the correlation between the preparation parameters and the MB adsorption capacity. Moreover, the residual diagnostic diagrams of the quadratic model are shown in Figs. 5b and c. Fig. 5b shows that the normal probability distribution of the residuals is approximately linear, which indicates that the distribution of data residuals is normal. And the irregular distribution of data residuals in Fig. 5c also proves that the established response quadratic model is reliable.

3.4. Response surface methodology plots

Among the preparation parameters, activation temperature (*C*) was found to have a more significant impact on the MB adsorption capacity due to the highest *F*-value of 183.59 as shown in Table 5. Besides, the interaction between impregnation mass ratio and activation time (*AD*), impregnation time and activation temperature (*BC*), impregnation time and activation time (*BD*), had an appreciable effect on MB adsorption capacity than the interaction between impregnation mass ratio and impregnation time (*AB*), impregnation mass ratio and activation temperature (*AC*), activation temperature and activation time (*CD*) (the *F*-value of *AD*, *BC* and *BD* is 22.78, 21.18 and 57.02, respectively). The results also can be seen from Figs. 6a–f, which indicates that the closer the contour is to the ellipse, the more obvious the interaction is.

Fig. 7a shows the combined effect of impregnation mass ratio and activation time on MB adsorption capacity with the impregnation time of 27 h and activation temperature of 600. It can be seen that the MB adsorption capacity increases firstly and then reduces with the increase of impregnation mass ratio, which indicates that the MB adsorption capacity becomes lower at lower and higher impregnation mass ratio. The roles of $ZnCl_2$ during the

Table 5
Analysis of variance (ANOVA) for quadratic model

Source	Sum of squares	df	Mean square	*F*-value	*p*-value	
Model	69,173.94	14	4,941.00	60.71	<0.0001	significant
A	3,491.84	1	3,491.84	42.90	<0.0001	significant
B	1,924.07	1	1,924.07	23.64	0.0003	significant
C	14,941.79	1	14,941.79	183.59	<0.0001	significant
D	482.47	1	482.47	5.93	0.0289	significant
AB	479.39	1	479.39	5.89	0.0293	significant
AC	875.27	1	875.27	10.75	0.0055	significant
AD	1,854.16	1	1,854.16	22.78	0.0003	significant
BC	1,723.91	1	1,723.91	21.18	0.0004	significant
BD	4,640.33	1	4,640.33	57.02	<0.0001	significant
CD	618.77	1	618.77	7.60	0.0154	significant
A^2	15,004.86	1	15,004.86	184.37	<0.0001	significant
B^2	6,459.73	1	6,459.73	79.37	<0.0001	significant
C^2	14,934.75	1	14,934.75	183.51	<0.0001	significant
D^2	21,304.45	1	21,304.45	261.77	<0.0001	significant
Residual	1,139.40	14	81.39			
Lack of fit	1,139.40	10	113.94			
Pure error	0.000	4	0.000			
Cor. total	70,313.34	28				

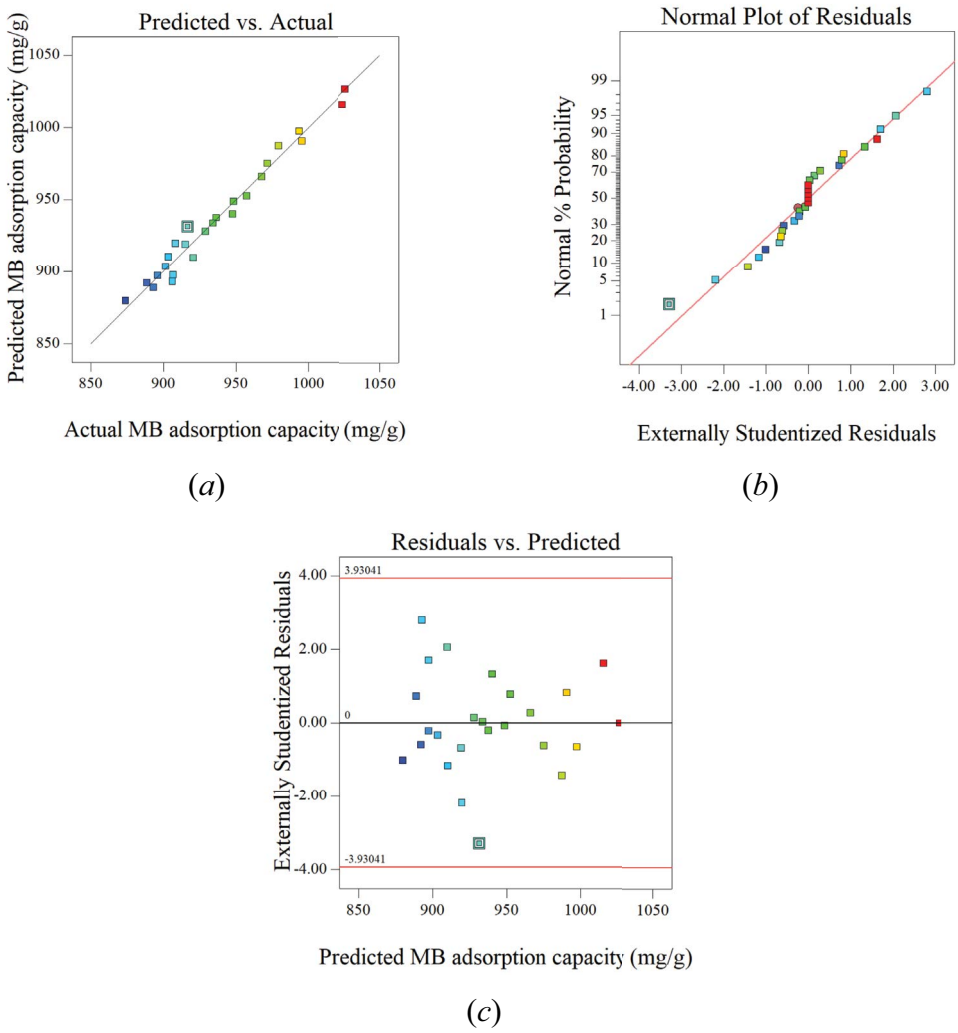

Fig. 5. Diagnostics of the prediction model.

carbonization process can be embodied from two aspects, catalytic dehydration and providing carbon skeleton. On the one hand, $ZnCl_2$ can catalyze dehydration at high temperatures, so that the hydrogen and oxygen atoms in the raw material can be separated in the form of water. Thus more carbon is retained in the raw material. On the other hand, $ZnCl_2$ can provide a skeleton, where the carbon can deposit on it during the carbonization process. Therefore, the developed carbon skeleton cannot be formed when the impregnation mass ratio is lower. Meanwhile, the developed microporous structure may be destroyed when the impregnation mass ratio is higher. Moreover, Fig. 6a shows that the MB adsorption capacity also improves when the activation time increases, but thereafter declines from its peaks. The decrease is possibly due to the developed porous structure may collapse as a result of sintering for a prolonged time. However, a reasonable extension of activation time is needed to enhance porosity and produce developed porous activated carbons.

Furthermore, the combined effect of impregnation time and activation temperature on MB adsorption capacity with impregnation mass ratio of 12.5 and activation time of 75 min is shown in Fig. 7b. The variation of MB adsorption capacity are consistent with that affected by impregnation mass ratio and activation time, that is, increases firstly and then declines. As described above, $ZnCl_2$ can remove the hydrogen and carbon atoms from raw materials and act as the carbon skeleton. Thus, the porous structure will be more developed with the increase of impregnation time. But the developed porous structure may collapse and results in the widening of micropores with a prolonged impregnation time. In addition, more volatile matters are released during the carbonization process before the activation temperature reaches the peak value, thereby more pores are developed, and then the MB adsorption capacity increases progressively. However, the reduction of MB adsorption capacity after the peak value can be due to the widening of micropores caused by excessive burn-off at higher temperatures. The widened micropores become mesopores or macropores, resulting in the significant reduction of the specific surface area of CnSACs and even the lack of well-developed pores. Overall, the MB adsorption capacity not only depends on the development of porous structure but also on the width of micropores.

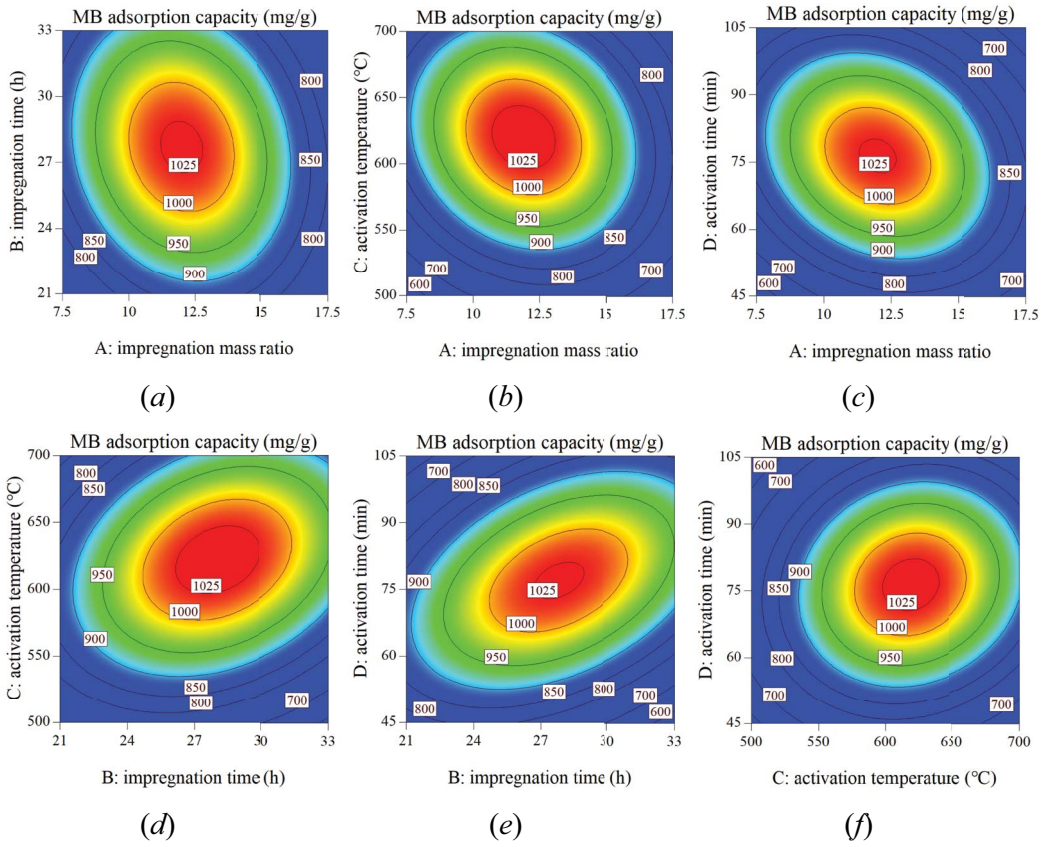

Fig. 6. Quadratic model contour plots of MB adsorption.

3.5. Optimization

To investigate the maximum MB adsorption capacity, optimization of the preparation parameters was carried out using numerical optimization methods. After the calculation, the optimum preparation parameters were found to be impregnation mass ratio of 11.363, impregnation time of 29.17 h, activation temperature of 632.42°C and activation time of 81.39 min. And the MB adsorption capacity of CnSAC prepared under the optimum preparation conditions was 1,047.75 mg/g predicted by the response quadratic model with desirability of 0.93. Then, an opt-CnSAC was prepared (impregnation mass ratio of 11.4, impregnation time of 29 h, activation temperature of 632°C and activation time of 81 min). The amount of MB absorbed onto the opt-CnSAC is 1,060.94 mg/g. Compared with the predicted values, the error is less than 1.3%, which indicates that the predicted values are in good agreement with the experimental values. Consequently, the quadratic model has sufficient accuracy to predict the MB adsorption capacity.

3.6. Characterization of CnSAC prepared under optimum preparation conditions

The N_2 adsorption isotherms of opt-CnSAC are shown in Fig. 8. With the increase of relative pressure (P/P_0), the smaller gas volume adsorbed increases sharply and then stabilizes. The relative pressure is around 0.4 at the turning point. Therefore, opt-CnSAC exhibits Type I isotherms, which also proves the conclusion that nitrogen molecules are adsorbed mainly in the microporous structure. Moreover, Table 6 shows the BET surface area, total pore volume, micropore volume and average pore diameter of opt-CnSAC. The results show that the micropore volume is about 96.4% of the total pore volume. Compared with the typical CnSACs in Section 3.1 (Table 3), the BET surface area and average pore diameter are all optimized. Moreover, we compared the BET surface area of activated carbons prepared from different sorts of biomass, which is shown in Table 7. The comparison indicates that the CnSAC has a bright application in the preparation of porous adsorption materials.

4. Conclusion

From the concept of treat waste with waste perspective, an activated carbon prepared from chestnut shell

Table 6
BET surface, total pore volume, micropore volume and average pore diameter of opt-CnSAC

BET surface area (m^2/g)	1,602.99
Total pore volume (cm^3/g)	0.84
Micropore volume (cm^3/g)	0.81
Average pore diameter (nm)	2.11

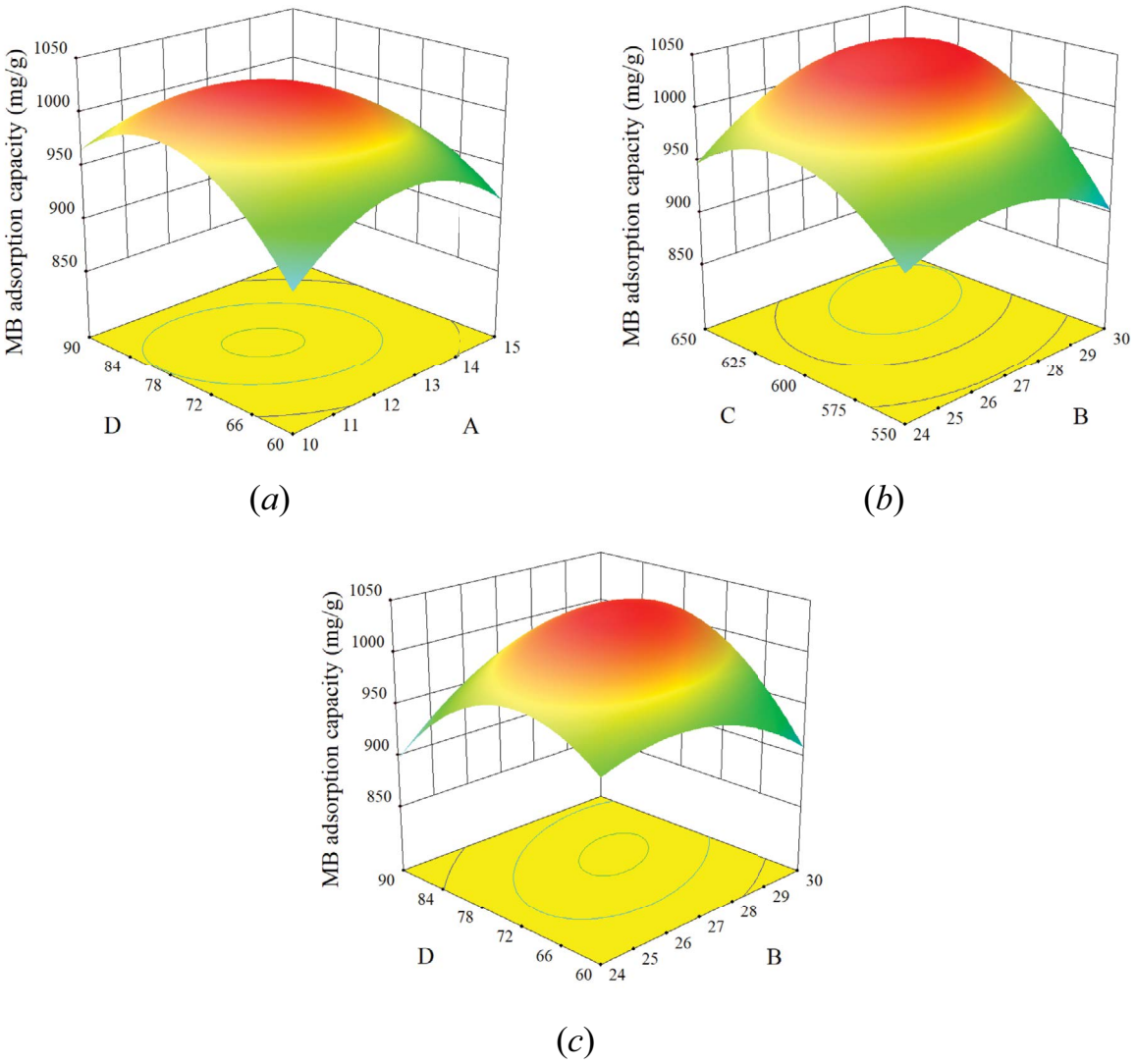

Fig. 7. Response surface plot of MB adsorption.

(CnSAC) was proposed in the present research. And the investigations of methylene blue (MB) adsorption from aqueous solution onto CnSACs were carried out. The SEM micrographs show that there are abundant abnormity protrusions, depressions and folds on the surface of CnSACs, which provide more adsorption sites for the adsorbate. And the N_2 adsorption–desorption isotherms indicate that the CnSACs exhibit Type I isotherms. Besides, response surface methodology (RSM) in combination with BBD was used to reveal the relationship between the preparation parameters and MB adsorption capacity. The results indicate that activation temperature is found to have a more significant impact on MB adsorption capacity than the other parameters. Moreover, the optimization of preparation parameters was carried out to investigate the maximum MB adsorption capacity. The BET surface area analysis of the activated carbon prepared under the optimum preparation parameters confirmes the development of a porous material with a BET surface area, total pore volume, micropore volume, and average pore diameter of 1602.99 m^2/g, 0.84 cm^3/g,

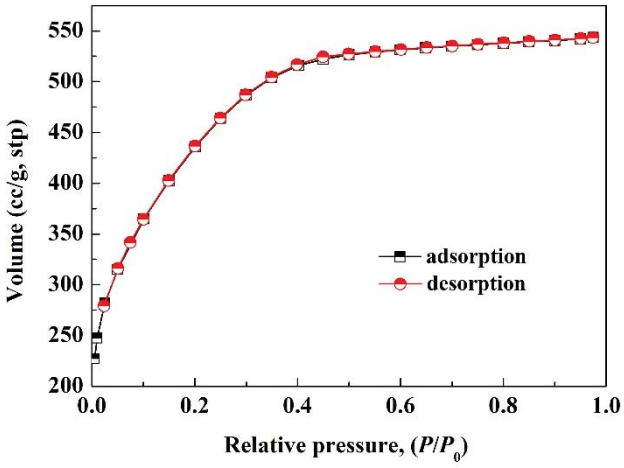

Fig. 8. The N_2 adsorption–desorption isotherms of opt-CnSAC (impregnation mass ratio of 11.4; impregnation time of 29 h; activation temperature of 632°C; activation time of 81 min).

Table 7
BET surface area of activated carbons

Raw material	BET surface area (m^2/g)	Reference
Chestnut shell	1,602.99	This paper
Camel bones	162	Alqadami et al. [7]
Amygdalus	209.74	Bagheri et al. [23]
Pine nut shell	266	Naushad et al. [25]
Pistachio shell	35.57	Khan et al. [26]
Palm shell	642	Arami-Niya et al. [33]
Waste rubber tires	468.98	Danmaliki et al. [34]
Pomegranate seeds	978.8	Uçar et al. [35]
Sugarcane bagasse	790	Tsai et al. [37]
Tectona grandis sawdust	585	Mohanty et al. [38]
Banana stem waste	267.54	Praveena et al. [40]
Tamarind wood	1,322	Sahu et al. [42]

0.81 cm^3/g and 2.11 nm, respectively. Therefore, it can be concluded that the CnSAC has a good potential to be used as a better alternative to commercial activated carbon for the removal of dyes from wastewaters.

Acknowledgments

The authors duly acknowledge the contributions of the School of Thermal Engineering, Shandong Jianzhu University, for providing all the basic laboratory facilities to accomplish the research work. And this work was supported by the Plan of Guidance and Cultivation for Young Innovative Talents of Shandong Province, the Doctoral Research Fund of Shandong Jianzhu University (X18068Z) and the Natural Science Foundation of Shandong Province (ZR2020QE204, ZR2019BEE023).

References

[1] K.Y. Foo, B.H. Hameed, An overview of dye removal via activated carbon adsorption process, Desal. Water Treat., 19 (2010) 255–274.
[2] A. Mittal, J. Mittal, A. Malviya, D. Kaur, V.K. Gupta, Adsorption of hazardous dye crystal violet from wastewater by waste materials, J. Colloid Interface Sci., 343 (2010) 463–473.
[3] M.A. Khan, Momina, M.R. Siddiqui, M. Otero, S.A. Alshareef, M. Rafatullah, Removal of rhodamine B from water using a solvent impregnated polymeric dowex 5WX8 resin: statistical optimization and batch adsorption studies, Polymers (Basel), 12 (2020) 500, doi: 10.3390/polym12020500.
[4] U. Filipkowska, E. Klimiuk, S. Grabowski, E. Siedlecka, Adsorption of reactive dyes by modified chitin from aqueous solutions, Pol. J. Environ. Stud., 11 (2002) 315–323.
[5] A.M. Aljeboree, A.F. Alkaim, A.H. Al-Dujaili, Adsorption isotherm, kinetic modeling and thermodynamics of crystal violet dye on coconut husk-based activated carbon, Desal. Water Treat., 53 (2014) 3656–3667.
[6] P. Kaur, A.P. Singh, A.K. Prince, J.P. Kushwaha, Optimization and evaluation of CBSOL LE red wool dye adsorption from aqueous solution onto commercial activated carbon, Int. J. Environ. Sci. Technol., 12 (2014) 3755–3766.
[7] A.A. Alqadami, M.A. Khan, M. Otero, M.R. Siddiqui, B.H. Jeon, K.M. Batoo, A magnetic nanocomposite produced from camel bones for an efficient adsorption of toxic metals from water, J. Cleaner Prod., 178 (2018) 293–304.
[8] H. Xu, B. Yang, Y.B. Liu, F. Li, C.S. Shen, C.Y. Ma, Q. Tian, X.S. Song, W.G. Sand, Recent advances in anaerobic biological processes for textile printing and dyeing wastewater treatment: a mini-review, World J. Microbiol. Biotechnol., 34 (2018) 165, doi: 10.1007/s11274-018-2548-y.
[9] S. Figueroa, L. Vázquez, A. Alvarez-Gallegos, Decolorizing textile wastewater with Fenton's reagent electrogenerated with a solar photovoltaic cell, Water Res., 43 (2009) 283–294.
[10] R.M. Simmons, S.M.R. Smith, M.P. Osborne, Methylene blue dye as an alternative to isosulfan blue dye for sentinel lymph node localization, Breast J., 7 (2001) 181–183.
[11] S.D. Khattri, M.K. Singh, Removal of malachite green from dye wastewater using neem sawdust by adsorption, J. Hazard. Mater., 167 (2009) 1089–1094.
[12] S. Papić, N. Koprivanac, A. Lončarić Božić, Removal of reactive dyes from wastewater using Fe(III) coagulant, Color. Technol., 116 (2000) 352–358.
[13] H.M. Zou, W.Z. Ma, Y. Wang, A novel process of dye wastewater treatment by linking advanced chemical oxidation with biological oxidation, Arch. Environ. Prot., 41 (2015) 33–39.
[14] S.H. Lin, C.C. Lo, Treatment of textile wastewater by foam flotation, Environ. Technol., 17 (1996) 841–849.
[15] M.F. Abid, M.A. Zablouk, A.M. Abid-Alameer, Experimental study of dye removal from industrial wastewater by membrane technologies of reverse osmosis and nanofiltration, Iran. J. Environ. Health Sci. Eng., 9 (2012) 17, doi: 10.1186/1735-2746-9-17.
[16] M.M. Hassan, C.M. Carr, A critical review on recent advancements of the removal of reactive dyes from dyehouse effluent by ion-exchange adsorbents, Chemosphere, 209 (2018) 201–219.
[17] T. Hudaya, J. Anthonios, E. Septianto, UV/Fenton photo-oxidation of Drimarene Dark Red (DDR) containing textile-dye wastewater, IOP Conf. Ser.: Mater. Sci. Eng., 162 (2016) 012022.
[18] Y. Xiong, P.J. Strunk, H.Y. Xia, X.H. Zhu, H.T. Karlsson, Treatment of dye wastewater containing acid orange II using a cell with three-phase three-dimensional electrode, Water Res., 35 (2001) 4226–4230.
[19] K. Pakshirajan, S. Kheria, Continuous treatment of coloured industry wastewater using immobilized *Phanerochaete chrysosporium* in a rotating biological contactor reactor, J. Environ. Manage., 101 (2012) 118–123.
[20] S. Şen, G. Demirer, Anaerobic treatment of real textile wastewater with a fluidized bed reactor, Water Res., 37 (2003) 1868–1878.
[21] E.-R. Kenawy, A.A. Ghfar, S.M. Wabaidur, M.A. Khan, M.R. Siddiqui, Z.A. Alothman, A.A. Alqadami, M. Hamid, Cetyltrimethylammonium bromide intercalated and branched polyhydroxystyrene functionalized montmorillonite clay to sequester cationic dyes, J. Environ. Manage., 219 (2018) 285–293.

[22] S.M. Wabaidur, M.A. Khan, M.R. Siddiqui, M. Otero, B.-H. Jeon, Z.A. Alothman, A.A.H. Hakami, Oxygenated functionalities enriched MWCNTs decorated with silica coated spinel ferrite – a nanocomposite for potentially rapid and efficient de-colorization of aquatic environment, J. Mol. Liq., 317 (2020) 113916, doi: 10.1016/j.molliq.2020.113916.
[23] S. Bagheri, M. Ghaedi, A. Asfaram, E.A. Dil, H. Javadian, RSM-CCD design of malachite green adsorption onto activated carbon with multimodal pore size distribution prepared from *Amygdalus scoparia*: kinetic and isotherm studies, Polyhedron, 171 (2019) 464–472.
[24] M.A. Khan, B.H. Hameed, J. Lawler, M. Kumar, B.H. Jeon, Developments in activated functionalized carbons and their applications in water decontamination: a review, Desal. Water Treat., 54 (2015) 422–449.
[25] Mu. Naushad, M.A. Khan, Z.A. Alothman, M.R. Khan, M. Kumar, Adsorption of methylene blue on chemically modified pine nut shells in single and binary systems: isotherms, kinetics, and thermodynamic studies, Desal. Water Treat., 57 (2016) 15848–15861.
[26] M.A. Khan, Z.A.A. Othman, M. Kumar, M.S. Ola, M.R. Siddique, Biosorption potential assessment of modified pistachio shell waste for methylene blue: thermodynamics and kinetics study, Desal. Water Treat., 56 (2015) 146–160.
[27] A.B. Pérez-Marín, V.M. Zapata, J.F. Ortuño, M. Aguilar, J. Sáez, M. Lloréns, Removal of cadmium from aqueous solutions by adsorption onto orange waste, J. Hazard. Mater., 139 (2007) 122–131.
[28] M. Kousha, S. Tavakoli, E. Daneshvar, A. Vazirzadeh, A. Bhatnagar, Central composite design optimization of Acid Blue 25 dye biosorption using shrimp shell biomass, J. Mol. Liq., 207 (2015) 266–273.
[29] S. Bajpai, S.K. Gupta, A. Dey, M.K. Jha, V. Bajpai, S. Joshi, A. Gupta, Application of central composite design approach for removal of chromium(VI) from aqueous solution using weakly anionic resin: modeling, optimization, and study of interactive variables, J. Hazard. Mater., 227–228 (2012) 436–444.
[30] G.E.P. Box, D.W. Behnken, Some new three level designs for the study of quantitative variables, Technometrics, 2 (1960) 455–475.
[31] K.D. Daniel, J.A. Ritter, Equilibrium theory analysis of a pressure-swing adsorption cycle utilizing an unfavorable Langmuir isotherm. 2. approach to periodic behavior, Ind. Eng. Chem. Res., 42 (2003) 3381–3390.
[32] P. Kowalczyk, A.P. Terzyk, P.A. Gauden, R. Leboda, E. Szmechtig-Gauden, G. Rychlicki, Z.Y. Ryu, H. Rong, Estimation of the pore-size distribution function from the nitrogen adsorption isotherm. Comparison of density functional theory and the method of Do and co-workers, Carbon, 41 (2003) 1113–1125.
[33] A. Arami-Niya, W.M.A.W. Daud, F.S. Mjalli, F. Abnisa, M.S. Shafeeyan, Production of microporous palm shell based activated carbon for methane adsorption: modeling and optimization using response surface methodology, Chem. Eng. Res. Des., 90 (2012) 776–784.
[34] G.I. Danmaliki, T.A. Saleh, A.A. Shamsuddeen, Response surface methodology optimization of adsorptive desulfurization on nickel/activated carbon, Chem. Eng. J., 313 (2017) 993–1003.
[35] S. Uçar, M. Erdem, T. Tay, S. Karagöz, Preparation and characterization of activated carbon produced from pomegranate seeds by $ZnCl_2$ activation, Appl. Surf. Sci., 255 (2009) 8890–8896.
[36] Q. Lu, Z. Wang, C.-Q. Dong, Z.-F. Zhang, Y. Zhang, Y.-P. Yang, X.-F. Zhu, Selective fast pyrolysis of biomass impregnated with $ZnCl_2$: furfural production together with acetic acid and activated carbon as by-products, J. Anal. Appl. Pyrolysis, 91 (2011) 273–279.
[37] W.T. Tsai, C.Y. Chang, M.C. Lin, S.F. Chien, H.F. Sun, M.F. Hsieh, Adsorption of acid dye onto activated carbons prepared from agricultural waste bagasse by $ZnCl_2$ activation, Chemosphere, 45 (2001) 51–58.
[38] K. Mohanty, D. Das, M.N. Biswas, Adsorption of phenol from aqueous solutions using activated carbons prepared from *Tectona grandis* sawdust by $ZnCl_2$ activation, Chem. Eng. J., 115 (2005) 121–131.
[39] Q.F. Yu, H.R. Zhao, H. Zhao, S.N. Sun, X. Ji, M. Li, Y.F. Wang, Preparation of tobacco-stem activated carbon from using response surface methodology and its application for water vapor adsorption in solar drying system, Sol. Energy, 177 (2019) 324–336.
[40] S.M. Praveena, U. Rashid, S.A. Rashid, Application of activated carbon from banana stem waste for removal of heavy metal ions in greywater using a Box–Behnken design approach, Environ. Technol., 41 (2020) 3363–3374.
[41] A.C. Lua, J. Guo, Activated carbon prepared from oil palm stone by one-step CO_2 activation for gaseous pollutant removal, Carbon, 38 (2000) 1089–1097.
[42] J.N. Sahu, J. Acharya, B.C. Meikap, Optimization of production conditions for activated carbons from tamarind wood by zinc chloride using response surface methodology, Bioresour. Technol., 101 (2010) 1974–1982.